



Crystalline Properties and Strain Relaxation Mechanism of CVD Grown GeSn

F. Gencarelli,^{a,b,z} B. Vincent,^a J. Demeulemeester,^c A. Vantomme,^c A. Moussa,^a A. Franquet,^a A. Kumar,^{a,c} H. Bender,^a J. Meersschant,^a W. Vandervorst,^{a,c} R. Loo,^{a,*} M. Caymax,^{a,*} K. Temst,^c and M. Heyns^{a,b}

^aImec, B-3001 Leuven, Belgium

^bMTM-Department, KU Leuven, B-3001 Leuven, Belgium

^cIKS, KU Leuven, B-3001 Leuven, Belgium

In this contribution, we discuss the crystalline properties of strained and strain-relaxed CVD-grown GeSn layers with Sn content in the range 6.4–12.6 at.%. A positive deviation from Vegard's law was observed and a new experimental bowing parameter was extracted for GeSn: $b_{\text{GeSn}} = 0.041 \text{ \AA}$ (in excellent agreement with recent theoretical predictions). The GeSn critical thickness for strain relaxation as a function of Sn concentration was determined, resulting in significantly higher values than those predicted by equilibrium models. A composition-dependent strain relaxation mechanism was also found, with the formation of an increasing density of GeSn pyramidal islands in addition to misfit dislocations at lower Sn concentration.

© 2013 The Electrochemical Society. [DOI: [10.1149/2.011304jss](https://doi.org/10.1149/2.011304jss)] All rights reserved.

Manuscript submitted December 5, 2012; revised manuscript received January 17, 2013. Published January 29, 2013. This was Paper 3213 presented at the Honolulu, Hawaii, Meeting of the Society, October 7-12, 2012.

$\text{Ge}_{1-x}\text{Sn}_x$ alloys are intriguing materials, with a potentially major impact on future-generation microelectronic and photonic applications due to a sizable improvement of the charge transport properties^{1,2} and to a transition to a direct bandgap semiconductor for sufficiently high Sn concentrations.³ In addition, the possibility to tune the lattice parameter and bandgap of GeSn by varying the alloy composition opens new routes for stress implementation⁴⁻⁶ and heterogeneous integration.⁷

In order to gain a better understanding of the fundamentals and the tailoring of the material properties, it is indispensable to accurately assess (i) the alloy composition x and (ii) its influence on the GeSn relaxed cubic lattice constant a_0^{GeSn} . Stoichiometric data would be assessable via X-ray diffraction if Vegard's law:⁸

$$a_0^{\text{Ge}_{1-x}\text{Sn}_x} = a_0^{\text{Ge}}(1-x) + a_0^{\text{Sn}}x + b^{\text{GeSn}}x(1-x) \quad [1]$$

(with the inclusion of an appropriate bowing parameter b^{GeSn} to account for deviations from a pure linear interpolation between the Ge and Sn lattice constants a_0^{Ge} and a_0^{Sn}) would correctly model the lattice constants as a function of composition - which is usually the case for compound semiconductors. Although various studies in literature theoretically predict a positive deviation from Vegard's law for GeSn,^{9,10} there is neither an experimental agreement on the sign nor on the magnitude of this deviation. For example, Chizmeshya et al.¹¹ and Chibane et al.⁹ observed both experimentally and theoretically a small and a strong positive deviation from Vegard's law for GeSn, respectively. Chibane et al. also extracted an experimental bowing parameter value $b^{\text{GeSn}} = 0.65 \text{ \AA}$, while Kouvetakis et al.¹ and Beeler et al.¹⁰ extracted $b^{\text{GeSn}} = 0.166 \text{ \AA}$ and $b^{\text{GeSn}} = 0.0468 \text{ \AA}$, respectively, from their experiments. These discrepancies, which are most probably due to experimental uncertainties in the alloy composition and strain level, prompted us to investigate the validity of Vegard's law for GeSn.

Another relevant obstacle to be solved in order to benefit from GeSn properties is that bulk GeSn alloys are not stable against Sn precipitation - due the limited (<1%) equilibrium solid solubility of Sn into the Ge matrix. However, *metastable* GeSn films can be epitaxially grown on crystalline Ge or Si substrates using adequate out-of-equilibrium growth techniques. The advantageous use of the resulting lattice-mismatched heterostructures requires a detailed knowledge and control of the specific strain relaxation mechanisms involved. For this purpose, the crystal structure and surface morphology of strained and strain-relaxed GeSn layers with different Sn contents are being systematically investigated and the first results are presented in this contribution.

Experimental

Metastable GeSn alloys were epitaxially grown on 200 mm Ge virtual substrates (i.e. $1 \mu\text{m}$ Ge/Si(001) substrates prepared as in¹²) by Reduced and Atmospheric Pressure Chemical Vapor Deposition (CVD)¹³ using an ASM Epsilon-like EPI reactor. An ex-situ HF (2%) wet etch and an in-situ H_2 preEPI bake at 40 Torr were performed on the Ge virtual substrates before GeSn growth in order to obtain clean, O and C free starting surfaces.

GeSn growth is challenged by the larger size and lower surface energy of Sn atoms (leading to their precipitation and surface segregation), and the high lattice mismatch (15%) between Ge and the diamond-cubic α -Sn structure (which is instable above 13.8°C). However, the low growth temperature of 320°C and the novel combination of SnCl_4 and Ge_2H_6 as the Sn and Ge precursors,¹⁴ respectively, allowed the incorporation of Sn contents exceeding 10% into GeSn.

The Sn content was determined by Rutherford backscattering spectrometry (RBS) - continuously rotating the samples during the measurements to avoid unintentional channeling - Energy-dispersive X-ray spectroscopy (EDS), Atom Probe Tomography (APT) and High-resolution X-ray diffraction reciprocal space mapping (HR-XRD RSM) of the asymmetric (224) Bragg reflection using Eq. 1. The latter technique was also used to extract the experimental in-plane and out-of-plane lattice constants, i.e. $a_{\parallel}^{\text{GeSn}}$ and a_{\perp}^{GeSn} .

Finally, HR-XRD RSM, scanning (SEM) and transmission (TEM) electron microscopy and atomic force microscopy (AFM) were used to study the crystal structure and surface morphology of GeSn layers as a function of Sn content - in the range 6.4–12.6 at.% - and film thickness - in the range 30–1000 nm (as determined from the thickness fringes visible in the XRD (004) 2θ - ω scans and confirmed by Scanning SEM / TEM inspection).

Vegard's Law for GeSn

In order to evaluate the validity of Vegard's law for GeSn and to accurately quantify possible small deviations from it, it is necessary to remove all the factors which might introduce experimental uncertainties or errors. Among those factors, an inexact knowledge of the alloy composition would have had negative effects on the reliability of our study. For this purpose, a cross calibration of different Sn content measurement techniques was first performed in order to develop a reliable probing procedure. In particular, the Sn content was primarily determined by RBS. Auger Electron Spectroscopy was also performed to verify the absence of light contaminants in GeSn (whose presence should have been included in the analysis of RBS spectra). In addition, RBS random and channeled spectra were compared in order to assess the substitutionality of Sn atoms in the Ge lattice. Since the vast majority of Sn atoms either occupies a substitutional or a random

*Electrochemical Society Active Member.

^zE-mail: Federica.Gencarelli@imec.be

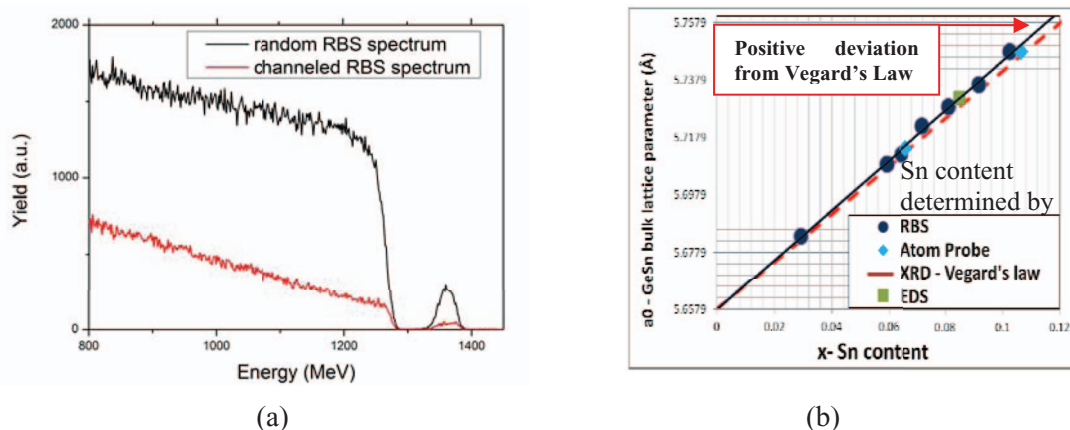


Figure 1. (a) Random and Channeled RBS spectra of a 40 nm thick $\text{Ge}_{0.92}\text{Sn}_{0.08}/\text{Ge}/\text{Si}(001)$ sample showing a high degree of channeling for both Ge and Sn in GeSn (indicating Sn substitutionality). (b) GeSn relaxed cubic lattice constant $a_0(x)$ as a function of the Sn content x determined by RBS (and confirmed by EDS and APT). The dashed line represents $a_0(x)$ as calculated from the pure Vegard's Law, the solid line is a fit of the HR-XRD RSM vs. RBS experimental data to Eq. 1.

interstitial lattice site,¹⁵ a channeling measurement along one direction is sufficient to estimate the substitutional fraction. The Sn and Ge signals coming from the GeSn layer showed the same ($\chi_{\min} < 10\%$) minimum channeling yield value (i.e. the ratio of channelled to random backscattering yield), as shown for a representative 40 nm thick $\text{Ge}_{0.92}\text{Sn}_{0.08}/\text{Ge}/\text{Si}(001)$ sample in Fig. 1a). This χ_{\min} value is noticeably low when taking into account that GeSn layer are grown on a virtual Ge substrate, which is a less perfect starting material as compared with a pure Ge substrate, and it indicates that nearly all Sn atoms reside in substitutional lattice sites.

Fig. 1b shows a summary of the Sn content values determined by RBS, EDS and APT. The latter, in particular, has a compositional sensitivity of the order of parts per million. The agreement among all the experimental data points (as evincible from their alignment in Fig. 1b), provided the necessary evidence for accurate alloy composition determination, independent of strain level.

The elastic constant ratio dependence on the Sn content x (determined by RBS) was assumed¹⁰ to be:

$$C_{12}/C_{11} = 0.3738 + 0.167x - 0.0296x^2 \quad [2]$$

in order to calculate the relaxed GeSn lattice constant as:

$$a_0^{\text{GeSn}} = (a_{\perp}^{\text{GeSn}} + 2a_{\parallel}^{\text{GeSn}} C_{12}/C_{11}) / (1 + 2C_{12}/C_{11}) \quad [3]$$

Fig. 1b shows the experimental GeSn relaxed cubic lattice constant $a_0^{\text{GeSn}}(x)$ as a function of the Sn content x determined by RBS, EDS and APT. The dashed line represents $a_0^{\text{GeSn}}(x)$ as calculated using the pure Vegard's Law, while the solid line is a fit of the HR-XRD RSM vs. RBS experimental data to Eq. 1. The total Sn concentration values detected by RBS, EDS and APT were lower than the substitutional ones measured by XRD using the pure Vegard's law. This illogical result clearly reveals that a positive deviation from Vegard's law must exist for GeSn. This behavior is in contrast with that of other group IV alloys, where a small negative deviation from Vegard's law is usually observed.¹⁶ However, this difference is in agreement with various ab initio theoretical studies (e.g. ^{11,16}).

A fit of the relaxed GeSn lattice constant $a_0^{\text{GeSn}}(x)$ as a function of the composition (x) measured by RBS using Equation 1 and leaving only b^{GeSn} as free parameter allowed the extraction of an experimental bowing parameter $b^{\text{GeSn}} = 0.041 \text{ \AA} \pm 0.014 \text{ \AA}$ (with 95% confidence, R-squared = 0.9974). This value was in excellent agreement with the theoretical value 0.0468 \AA recently calculated by Beeler et al.¹⁰ using Density Functional Theory. We note that Beeler observed a negative experimental bowing parameter (-0.066 \AA) using a comparable Sn content range and experimental technique as in this work, but without proposing a conclusive explanation for this discrepancy. In our opinion, this confirms that very accurate Sn content measurements are mandatory to investigate such small deviations from Vegard's law.

GeSn Strain Relaxation Mechanism

Cross-sectional TEM images revealed that fully strained, defect-free single-crystal GeSn layers grew epitaxially on Ge. Their good crystalline quality was also confirmed by the symmetrical line shapes and the small full width at half maximum values (0.080° – 0.120°) of the corresponding GeSn peaks in the XRD (004) 2θ - ω scans (not shown).

Fig. 2a contains a summary of the (224) GeSn reciprocal lattice points measured by HR-XRD RSM showing the crystallographic evolution of the as-grown GeSn layers with different Sn contents (6.4–10.5%) as a function of increasing thickness (30–1000 nm) and subsequent increasing strain relaxation degree (0–75%). The dotted lines represent the calculated reciprocal lattice points of strain-relaxing GeSn crystals complying with [1]. As expected,¹ we always observed $a_{\perp}^{\text{GeSn}} \geq a_{\parallel}^{\text{GeSn}}$ due to the tetragonal distortion undergone by the biaxially compressively strained GeSn lattice growing on Ge(001) ($a_0^{\text{Ge}} < a_0^{\text{GeSn}}$). It can be noticed that, when the layer thickness is increased while leaving the alloy composition unchanged, a process of strain relaxation occurs, with a_{\perp}^{GeSn} and $a_{\parallel}^{\text{GeSn}}$ changing continuously toward the bulk lattice parameter $a_0^{\text{GeSn}}(x)$. A deviation from this continuous trend is noticeable for 10.5% GeSn layers due to non-uniform growth rate and Sn incorporation. In order to confirm this, a fully strained layer and a 75% strain relaxed layer (indicated by S and R, respectively, in Fig. 2) with the same nominal Sn content of 10.5% Sn were compared. Differential mass measurements revealed a higher growth rate for the fully strained layer as compared to the relaxed one ($\text{GR}_S = 57 \text{ nm/min} > \text{GR}_R = 47 \text{ nm/min}$). In addition, Secondary Ions Mass Spectrometry (SIMS) analysis of sample R (shown in Fig. 2b) indicated a lower Sn content at the beginning of the growth, i.e. at the same thickness of sample S ($\text{Sn}_S = 10.5\% < \text{Sn}_R = 12.6\%$, as determined by RBS).

The first outcome of this study was the determination of the critical GeSn thickness of strain relaxation (h_c), above which it becomes energetically favorable for misfit dislocations (MDs) to be formed at the GeSn/Ge interface in order to relax the tetragonally distorted compressively strained GeSn epilayer. For each Sn content, h_c was determined from Fig. 2 in correspondence of the first 224 XRD GeSn peak appreciably departing from the vertical pseudomorphic line (the latter indicating the locus of the reciprocal space points with the same in-plane lattice constant as the underlying Ge layer). Fig. 3a shows the measured h_c values as a function of the GeSn/Ge misfit, for Sn contents in the range 6.4–10.5%. The graph also shows the h_c values as predicted by the Matthews and Blakeslee¹⁷ and Frank and Van der Merwe¹⁸ equilibrium models – assuming a Burgers vector $b = 4 \text{ \AA}$ (corresponding to 60° dislocations) and a Poisson ratio $\nu = 0.263$. It can be observed that our experimental h_c values considerably exceed the equilibrium predictions. This means that the

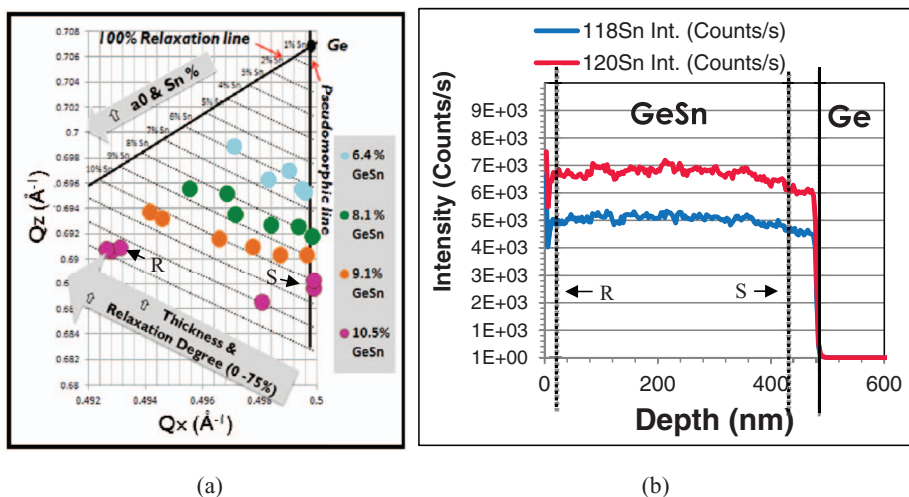


Figure 2. (a) Measured 224 reciprocal lattice points of GeSn layers with Sn content in the range 6.4–10.5% and strain relaxation degree ranging from 0 to 75%. The dotted lines represent the calculated reciprocal lattice sites of strain-relaxing GeSn crystals. (b) SIMS Sn profile in a 75% GeSn layer with nominal Sn content of 10.5% Sn (labeled as R in Fig. 2a).

GeSn layers grown under such conditions (i.e. low T CVD⁶) are in a metastable state, where kinetic barriers¹⁹ have likely delayed the formation and/or motion of misfit dislocations (MDs).

Fig. 3b shows the TEM image of the full stack of a representative ~50% relaxed GeSn layer (240 nm thick) with 8.1% Sn, acquired along the [110] zone axis; the inset shows a zoom of the Ge/GeSn image taken in (220) 2-beam conditions which improves the contrast at the dislocations. The GeSn surface is flat and a MD network can be observed at GeSn/Ge interface. Threading dislocations (TDs) are also observed about 50–100 nm above the GeSn/Ge interface: these might be bended TDs, likely resulting from TDs glide and reaction, belonging to a confined dislocation network as the one observed at 50 nm from the Ge/Si interface for CVD grown Ge layers after TDD anneal.²⁰

Most importantly, a composition-dependent strain relaxation mechanism was found in this study. At higher misfits (i.e. higher Sn concentration), a more classical behavior was observed, with the formation of a MD network at the GeSn/Ge interface (as in Fig. 3b), beyond the abovementioned critical thickness for plastic relaxation h_c . In those cases, a corresponding cross-hatch pattern was observed on the surface.

At lower misfits, a progressively stronger islanding tendency was also observed to contribute to the strain relaxation of the growing layer in combination with the MDs network. In fact, GeSn layers with lower Sn contents were characterized by an increase in island density and size as the strain relaxation degree increased, as shown by the AFM pictures in Fig. 4a of 8% (a1), 33% (a2) and 75% (a3) strain relaxed GeSn layers with 6.4% Sn content. The islands observed on these layers have a square-based pyramidal shape and a contact angle increasing from 7.5° and 15° (from {108} to {115} facets). In

analogy with the morphological evolution of the early stages of island growth in GeSi on Si,²¹ the increasing strain energy density at the island sides might continuously decelerate the lateral growth velocity, while adatoms would be preferentially incorporated on top of the elastically strain-relaxed islands, resulting in a growth rate increase in the vertical direction which would explain the observed increase in the contact angles of the facets. This increase is expected to stop when complete strain relaxation is reached and low energy facets are formed.

It was also observed by AFM that the islands sides were aligned along <110> directions, which correspond to the cross-hatch pattern line directions. This observation suggests that the GeSn islands have a direct correlation with the misfit dislocations at the GeSn/Ge interface. This can be attributed to two different reasons: (i) the higher strain energy density at the islands sides might favor the nucleation of new dislocations at the growing surface²² (which would then propagate to the interface) or (ii) the Ge and Sn adatoms could be preferentially incorporated on local lower energy surface sites caused by the inhomogeneous strain field associated with preexisting misfit dislocations (e.g. on regions with a locally larger lattice parameter²³ or at slip steps at the intersection of a dislocation glide plane with the film surface²⁴).

The formation of pyramidal islands was also observed during the growth of GeSn on Ge(001) substrates by Molecular Beam Epitaxy (at 155°C and 5E-11 Torr) by Bratland et al.²⁵ In that case the propensity toward faceting was enhanced with higher Sn content due to the related stronger effect of strain-induced roughening. Bratland et al. also pointed out that Sn atoms acted as surfactants: they smoothed the GeSn surface enhancing both Ge diffusivity on each terrace and toward lower terraces. However, this was true only at lower concentrations (<2%), above which the aforementioned strain-induced

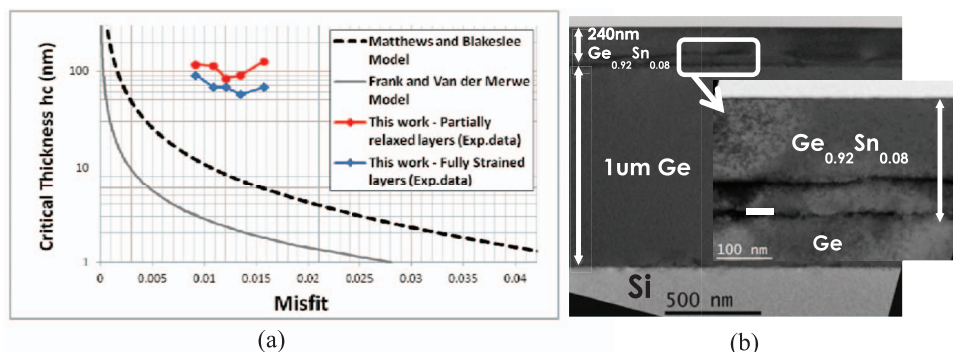


Figure 3. (a) GeSn critical thickness for plastic relaxation (h_c) as a function of GeSn/Ge misfit (6.4–10.5%Sn), compared with equilibrium predictions^{17,18} (b) TEM picture of ~50% relaxed GeSn layer with 8.1% Sn.

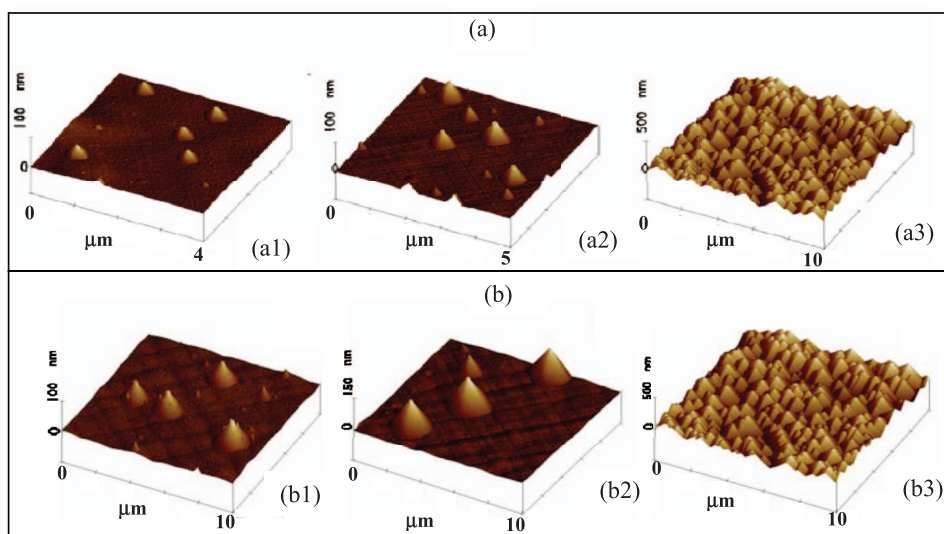


Figure 4. AFM pictures of (a) 6.4% GeSn layers with 8% (a1), 33% (a2) and 75% (a3) strain relaxation and (b) \sim 75% strain relaxed GeSn layers with 12.6% (b1), 8.1% (b2) and 6.4% (b3) Sn content.

roughening became dominant. An opposite behavior was observed in our work: the island density increased at lower Sn contents for GeSn layers with comparable strain relaxation degrees. This is shown by the AFM images of \sim 75% strain relaxed GeSn layers in Fig. 4a, containing Sn concentrations of 12.6% (b1), 8.1% (b2) and 6.4% (b3), respectively. This difference is expected to arise from the existence of kinetic barriers delaying island formation.²⁶ In order to understand their physical origin, it must be noticed that the GeSn layers with higher Sn concentration were grown using higher amounts of the Sn precursor (SnCl_4). Therefore, they were inevitably exposed to higher Cl doses. As a consequence, Ge dangling bonds were (more) saturated with Cl atoms, which likely changed the relative surface energies and/or inhibited Ge/Sn diffusion, as observed in.²⁷ It is then believed that Cl atoms acted as additional surfactants mediating GeSn morphological evolution together with Sn atoms. However, a lower surface energy made Cl atoms float on the growth surface without significant incorporation.

Conclusions

In summary, the GeSn crystalline properties were investigated and a positive deviation from Vegard's law was observed, resulting in the extraction of a new experimental bowing parameter for GeSn of $b_{\text{GeSn}} = 0.041 \text{ \AA}$, in excellent agreement with recent DFT predictions ($b_{\text{GeSn}} = 0.0468 \text{ \AA}$,¹⁰). In addition, the GeSn critical thickness for strain relaxation has been determined for different Sn concentration, resulting in significantly higher values than those predicted by equilibrium models. Finally, a composition-dependent strain relaxation mechanism was observed, with the formation of an increasing density of GeSn pyramidal islands in addition to misfit dislocations at lower Sn concentration. Possible reasons behind this difference were proposed, but further investigation of this specific GeSn growth-relaxation behavior are currently ongoing.

Acknowledgments

The authors gratefully acknowledge the imec core partners within the Imec Industrial Affiliation Program on Logic and the FP7 Integrated Infrastructure Initiative SPIRIT (contract 227012). Furthermore, we thank Voltaix and Dow for providing Ge_2H_6 and SnCl_4 , respectively, to imec. Finally, parts of this work frame within a collaboration funded by the Fund for Scientific Research-

Flanders (FWO) and the Japan Society for the Promotion of Science (JSPS).

References

1. J. Kouvetakis, J. Menendez, and A. V. G. Chizmeshya, *Annu. Rev. Mater. Res.*, **36**, 497 (2006).
2. D. W. Jenkins and J. D. Dow, *Phys. Rev. B*, **36**, 7994 (1987).
3. G. He and H. A. Atwater, *Phys. Rev. Lett.*, **79**, 1937 (1997).
4. S. Takeuchi, Y. Shimura, O. Nakatsuka, S. Zaima, M. Ogawa, and A. Sakai, *Appl. Phys. Lett.*, **92**, 231916 (2008).
5. C. Merckling, X. Sun, Y. Shimura, A. Franquet, B. Vincent, S. Takeuchi, W. Vandervorst, O. Nakatsuka, S. Zaima, R. Loo, and M. Caymax, *Appl. Phys. Lett.*, **98**, 192110 (2011).
6. B. Vincent, F. Gencarelli, D. Lin, L. Nyns, O. Richard, H. Bender, B. Douhard, A. Moussa, C. Merckling, L. Witters, W. Vandervorst, R. Loo, M. Caymax, and M. Heyns, *ECS Trans.*, **41**, 239 (2011).
7. R. Roucka, J. Tolle, C. Cook, A. V. G. Chizmeshya, J. Kouvetakis, V. D'Costa, J. Menendez, Z. D. Chen, and S. Zollner, *Appl. Phys. Lett.*, **86**, 191912 (2005).
8. L. Vegard, *Z. Phys.*, **5**, 17 (1921).
9. Y. Chibane and M. Ferhat, *J. Appl. Phys.*, **107**, 053512 (2010).
10. R. Beeler, R. Roucka, A. V. G. Chizmeshya, J. Kouvetakis, and J. Menendez, *Phys. Rev. B*, **84**, 035204 (2011).
11. A. V. G. Chizmeshya, M. R. Bauer, and J. Kouvetakis, *Chem. Mater.*, **15**, 2511 (2003).
12. R. Loo, G. Wang, L. Souriau, J. C. Lin, S. Takeuchi, G. Brammert, and M. Caymax, *J. Electrochem. Soc.*, **157**(1), H13 (2010).
13. B. Vincent, F. Gencarelli, H. Bender, C. Merckling, B. Douhard, D. H. Petersen, O. Hansen, H. H. Henriksen, J. Meererschaut, W. Vandervorst, M. Heyns, R. Loo, and M. Caymax, *Appl. Phys. Lett.*, **99**, 152103 (2011).
14. F. Gencarelli, B. Vincent, L. Souriau, O. Richard, W. Vandervorst, R. Loo, M. Caymax, and M. Heyns et al., *Thin Solid Films*, **520**, 3211 (2012).
15. S. Decoster, S. Cottelier, U. Wahl, J. G. Correia, and A. Vantomme, *Phys. Rev. B*, **81**, 155204 (2010).
16. E. Kasper, A. Schuh, G. Bauer, B. Holländer, and H. Kibbel, *J. Cryst. Growth*, **157**, 68 (1995).
17. J. W. Matthews and A. E. Blakeslee, *J. Cryst. Growth*, **27**, 118 (1974).
18. C. Frank and J. H. van der Merwe, *Proc. R. Soc. London*, Ser. A, 198 (1949).
19. R. Hull, J. C. Bean, D. J. Werder, and R. E. Leibenguth, *Phys. Rev. B*, **40**, 1681 (1989).
20. G. Wang, R. Loo, S. Takeuchi, L. Souriau, J. C. Lin, A. Moussa, H. Bender, B. De Jaeger, P. Ong, W. Lee, M. Meuris, M. Caymax, W. Vandervorst, B. Blanpain, and M. M. Heyns, *Thin Solid Films*, **518**, 2538 (2010).
21. W. Dorsh, S. Christiansen, M. Albrecht, P. O. Hansson, E. Bauser, and H. P. Strunk, *Surface Science*, **331**, 896 (1995).
22. S. Guha, A. Madhukar, and K. C. Rajkumar, *Appl. Phys. Lett.*, **57**, 2110 (1990).
23. B. Voigtlander and N. Theuerkauf, *Surface Science*, **461**, L575 (2000).
24. S. Yu. Shiryayev, F. Jensen, J. L. Hansen, J. W. Petersen, and A. N. Larsen, *Phys. Rev. Lett.*, **78**, 503 (1997).
25. K. A. Bratland, Y. L. Foo, T. Spila, H.-S. Seo, R. T. Haasch, P. Desjardins, and J. E. Greene, *J. Appl. Phys.*, **97**, 044904 (2005).
26. C. W. Snyder, J. F. Mansfield, and B. G. Orr, *Phys. Rev. B*, **46**, 9551 (1992).
27. T. I. Kamins, G. A. D. Briggs, and R. Stanley Williams, *Appl. Phys. Lett.*, **73**, 1862 (1998).